Reactive and Functional Polymers 123 (2018) 70–79

Contents lists available at ScienceDirect

Reactive and Functional Polymers

journal homepage: www.elsevier.com/locate/react

Hybrid cross-linked poly(2-acrylamido-2-methyl-1-propanesulfonic acid) hydrogels with tunable viscoelastic, mechanical and self-healing properties

Esra Su, Oguz Okay*

Istanbul Technical University, Department of Chemistry, 34469 Istanbul, Turkey

ARTICLE INFO

Keywords:
2-Acrylamido-2-methyl-1-propanesulfonic acid (AMPS)
Hydrogels
Laponite
Hybrid-cross-linking
Self-healing

ABSTRACT

Hydrogels derived from 2-acrylamido-2-methyl-1-propanesulfonic acid (AMPS) monomer are attractive materials for producing soft-biomimetic actuators, superabsorbents, and biomaterials. Here we present a simple synthetic strategy to prepare mechanically strong poly(2-acrylamido-2-methyl-1-propanesulfonic acid) (PAMPS) hydrogels with self-healing ability. Initiator-free polymerization of AMPS in aqueous solution in the presence of Laponite nanoparticles and *N,N′*-methylenebis(acrylamide) (BAAm) cross-linker produces hybrid-cross-linked hydrogels with excellent mechanical properties. The hydrogels exhibit a high modulus (~700 kPa), compressive strength (45 MPa at ~90% strain), good resilience, and self-healing. The results reveal that the incorporation of Laponite and BAAm separately into the physical PAMPS network weakens hydrogen bonding interactions while their combination enhances these interactions and generate water-insoluble hydrogels with a high modulus. The superior properties of hybrid cross-linked hydrogels are attributed to strengthening of the interactions between chemically cross-linked PAMPS chains and nanoparticles. The hybrid approach presented here might enable preparation of mechanically strong nanocomposite hydrogels consisting of strongly or weakly charged polymer chains of different architecture.

1. Introduction

2-Acrylamido-2-methyl-1-propanesulfonic acid (AMPS) is an ionic monomer widely used for the synthesis of polyelectrolyte hydrogels possessing a large water sorption capacity [1–4]. AMPS has received attention due to its strongly ionizable sulfonate group (Scheme 1); it dissociates completely in the overall pH range [5–7], and therefore, chemically cross-linked hydrogels derived from AMPS exhibit pH independent swelling behavior and good electro-responsive property making them attractive material in a wide range of applications, such as in soft-biomimetic actuators, superabsorbents, biomaterials, bioengineering, water purification, agriculture, and food industry [3,8–11]. However, such hydrogels have a low strength and toughness due to the lack of an effective energy dissipation mechanism [12–15].

Xing et al. recently reported preparation of a self-healing hydrogel based on PAMPS using initiator-free polymerization of AMPS in aqueous solutions in the absence of a cross-linker [16]. Their results indicate that the polymerization ability of AMPS in the absence of an external initiator is due to the catalytic effect of H^+ counterions of the sulfonic acid groups, while its self-cross-linking ability arises due to the intermolecular hydrogen bonds acting as physical cross-links [16]. This simple, inexpensive, and one-pot synthetic procedure leads to the formation of PAMPS hydrogels with mechanical properties strongly dependent on their water contents. For instance, the hydrogels containing < 10% water exhibit a Young's modulus approaching to 400 MPa, while increasing water content above 15% produces mechanically weak hydrogels with a modulus of around 22 kPa [16]. Our preliminary experiments showed that PAMPS hydrogels prepared as described by Xing et al. completely dissolve in excess of water indicating that the inter-chain hydrogen bonds are too weak to resist the expansion of PAMPS chains in water due to the osmotic pressure of AMPS counterions.

In this study, we attempt to improve the mechanical performance of physical PAMPS hydrogels using three strategies, as schematically illustrated in Scheme 1. First, Laponite nanoparticles were incorporated into the physical network of PAMPS chains to increase the strength of intermolecular interactions. Laponite is a synthetic hectorite clay and, when suspended in water, it forms disk-like particles with a thickness of 1 nm, a diameter of about 25 nm, carrying strongly negative charge on the surface and weakly positive charge on the rim (Scheme 1) [17,18]. At a low concentration, Laponite forms a clear colloidal suspension in water due to the repulsive electrostatic interactions between particle surfaces. Increasing Laponite concentration leads to the formation of a clay hydrogel with so-called house-of-cards structure due to the

* Corresponding author.
E-mail address: okayo@itu.edu.tr (O. Okay).

https://doi.org/10.1016/j.reactfunctpolym.2017.12.009
Received 26 September 2017; Received in revised form 9 December 2017; Accepted 17 December 2017
Available online 19 December 2017
1381-5148/

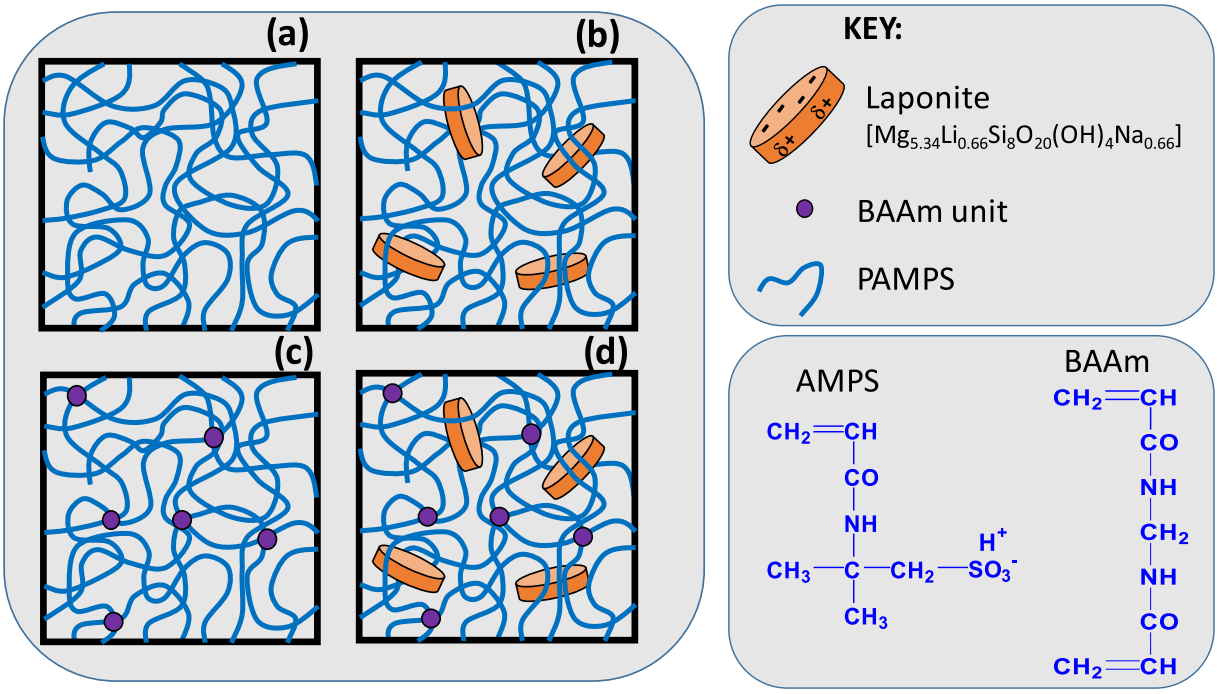

Scheme 1. Scheme of pure PAMPS (a), nanocomposite- (b), chemically-cross-linked- (c), and hybrid-cross-linked PAMPS hydrogels (d).

Table 1
Synthesis conditions, gel fractions W_g, storage modulus G' and loss factor tan δ, both measured at 1 and 100 rad·s^{-1}, and water contents of equilibrium swollen hydrogels. Standard deviations in the water contents are < 1% while for G' and tan δ, they are < 5%.

Code	AMPS/g	H_2O/g	Laponite/g	BAAm/mg	AMPS wt%	Laponite wt%	BAAm mol%	W_g	H_2O wt%	G'/kPa		tan δ	
										1 rad·s^{-1}	100 rad·s^{-1}	1 rad·s^{-1}	100 rad·s^{-1}
PAMPS	5	5	0		50	0		0	–	8	18	0.38	0.25
NC-1	5	5	0.10		50	1		0	–	10	23	0.38	0.23
NC-5	5	5	0.53		50	5		0	–	9	21	0.44	0.23
NC-10	5	5	1.10		50	10		0	–	14	36	0.47	0.30
NC-15	5	5	1.765		50	15		0	–	13	43	0.62	0.35
BAAm-0.5	5	5		20	50		0.5	0	–	10	24	0.39	0.28
BAAm-1	5	5		39	50		1	0	–	9	21	0.39	0.28
BAAm-1.3	5	5		49	50		1.3	0	–	10	19	0.27	0.23
BAAm-2	5	5		78	50		2	1.0 ± 0.1	99.7	14	21	0.12	0.16
Hybrid-15/0.5	5	5	1.765	20	50	15	0.5	0.90 ± 0.01	93	37	55	0.077	0.37
Hybrid-15/1	5	5	1.765	39	50	15	1	0.90 ± 0.01	90	57	77	0.079	0.31
Hybrid-15/1.3	5	5	1.765	49	50	15	1.3	0.95 ± 0.01	87	70	117	0.095	0.49
Hybrid-15/2	5	5	1.765	78	50	15	2	0.96 ± 0.03	86	38	67	0.11	0.54

electrostatic bonds between the positively charged rim and the negatively charged surfaces. Laponite nanoparticles have been used in many studies along with in-situ produced hydrophilic non-ionic polymers to form nanocomposite hydrogels with improved mechanical properties [19–22]. The surface of the nanoparticles provides an interface on which polymer chains can physically absorb, thus acts as multi-functional cross-link zones of nanocomposite hydrogels. Hydrogen bonding, ionic, dipole interactions and polymer entanglements seem to be responsible for the formation of nanocomposite hydrogels. As a second strategy, we included the classical chemical cross-linker *N*,*N*′-methylenebis(acrylamide) (BAAm) into the gelation solution to improve the elastic properties of the hydrogels.

As will be seen below, incorporation of Laponite (1–15 wt%) or BAAm (0.5–1.3 mol%) into the gelation system leads to the formation of water-soluble gels, as the pure PAMPS hydrogel, due to the weak inter-chain hydrogen bonds. However, simultaneous incorporation of Laponite and BAAm into the network structure strengthens hydrogen bonding interactions and provides formation of water-insoluble, hybrid cross-linked PAMPS hydrogels with excellent mechanical properties. For instance, they exhibit a high modulus (~700 kPa), compressive strength (45 MPa at ~90% strain), good resilience, and self-healing. Because nanocomposite polyelectrolyte hydrogels are hard to prepare due to agglomeration of the particles, the hybrid-cross-linking approach presented here might enable preparation of a variety of mechanically strong nanocomposite hydrogels consisting of charged polymer chains of different architecture.

2. Materials and methods

2.1. Materials

The monomer 2-acrylamido-2-propane-1-sulfonic acid (AMPS,

Aldrich), chemical cross-linker *N,N′*-methylenebis(acrylamide) (BAAm, Merck), and the synthetic hectorite clay, Laponite XLG ($Mg_{5.34}Li_{0.66}Si_8O_{20}(OH)_4Na_{0.66}$) provided by Rockwood Ltd. were used without further purification. The hydrogels were prepared by solution polymerization of AMPS at 80 °C in the absence of an external initiator. AMPS concentration was fixed at 50 wt%, with respect to water, while various amounts of Laponite and BAAm separately or together were added into the solution to obtain nanocomposite-, chemically cross-linked-, and hybrid-cross-linked hydrogels, respectively (Table 1). The concentration of Laponite is expressed as wt% of the solution while BAAm content is given by mol% with respect to the monomer AMPS. Typically, AMPS (5 g) was dissolved in 5 mL distilled water at 24 ± 2 °C. Laponite (0.10–1.765 g) was then added and stirred 2 h to obtain a homogeneous solution. We have to note that Laponite dissolved easier in the AMPS solution than in water, which is in accord with the dispersion effect of AMPS on Laponite aggregates [23]. After addition of BAAm (20–78 mg) and bubbling nitrogen, the solution was transferred into plastic syringes of 20 mm in diameter and the polymerization was conducted at 80 °C for 18 h.

2.2. Rheological experiments

Rheological measurements were performed on Gemini 150 Rheometer system, Bohlin Instruments, equipped with a Peltier device for temperature control. Hydrogel samples after preparation were cut into thin slices of 20 mm in diameter and about 3 mm in thickness and then placed between the parallel plates of the rheometer. The upper plate (diameter 20 mm) was set at a distance of 2950 ± 150 μm. During all measurements, a solvent trap was used to minimize the evaporation. The frequency-sweep tests at a strain amplitude $\gamma_o = 0.01$ were carried out at both 25 and 40 °C over the frequency range 0.1 to 300 rad·s^{-1}. The hydrogels were also subjected to stress-relaxation experiments at 25 °C. A shear deformation of predetermined strain amplitude γ_o was applied to the hydrogel samples and the resulting stress $\sigma(t, \gamma_o)$ was monitored as a function of time. Here, we report the relaxation modulus $G(t)$ as functions of the relaxation time t and strain amplitude γ_o. The experiments were conducted with increasing strain amplitudes γ_o from 0.01 to 1. For each hydrogel, stress-relaxation experiments at various γ_o were conducted starting from a value of the relaxation modulus deviating < 10% from the modulus measured at $\gamma_o = 0.01$.

2.3. Mechanical tests

Uniaxial compression and elongation tests were performed at 24 ± 2 °C on a Zwick Roell Z0.5 TH test machine using a 500 N load cell. Load and displacement data were collected using flat hydrogel samples with dimensions of 4 × 3 mm and a thickness of 3 mm. For uniaxial compression measurements, the hydrogel samples were compressed at various strain rates $\dot{\varepsilon}$ between 0.1 and 4 min^{-1}. Before the test, an initial compressive contact to 0.01 N was applied to ensure a complete contact between the gel and the plates. For uniaxial elongation measurements, the initial sample length between jaws and the strain rate were 10 ± 1 mm and 1 min^{-1}, respectively. The stress was presented by its nominal σ_{nom} and true values σ_{true} ($= \lambda\sigma_{nom}$), which are the forces per cross-sectional area of the undeformed and deformed specimen, respectively, while the strain is given by λ, the deformation ratio (deformed length/initial length). The strain ε is also defined as the change in the length of the gel specimen relative to its initial length, i.e., $\varepsilon = \lambda - 1$ or $\varepsilon = 1 - \lambda$, for elongation and compression, respectively. The Young's modulus E was calculated from the slope of nominal stress–strain curves between 5 and 15% deformations. The compressive strength σ_f was calculated from the maxima in true stress-strain curves [24]. Cyclic compression experiments were conducted with a compression step performed at a strain rate $\dot{\varepsilon}$ of 1 min^{-1} to a maximum strain ε_{max} (increased from 0.2 to 0.8), followed by immediate retraction to zero displacement and a waiting time of 5 min, until the next cycle of compression.

To quantify the healing efficiency, tensile testing experiments were performed using cylindrical gel samples of 4.6 mm in diameter and 1 cm in length. The samples were cut in the middle and then, the two halves were merged together within a plastic syringe (of the same diameter as the gel sample) by slightly pressing the piston plunger. The healing time was fixed at 24 h. Healing efficiency ε_{eff} was estimated from the ratio of the Young's modulus and fracture stress of the healed samples to those of the virgin sample.

2.4. Swelling and gel fraction measurements

The hydrogel samples after preparation were cut into specimens of about 3 mm in length. Then, each specimen was immersed in a large excess of distilled water at 24 ± 2 °C for at least 6 days by replacing water every hour during the first 6 h of the swelling period and then every day to extract any soluble species. The swelling equilibrium was tested by weighing the gel samples. The equilibrium swollen hydrogel samples in distilled water were than taken out of water and freeze dried. The gel fraction W_g, that is, the fraction of AMPS, BAAm, and Laponite incorporated into the water-insoluble polymer was calculated from the masses of dry polymer network and from the comonomer feed. The relative weight swelling ratio m_{rel} was calculated as $m_{rel} = m/m_o$ where m is the mass of the equilibrium swollen gel sample, and m_o is its mass after preparation. The water content H_2O % of the hydrogels was calculated as $H_2O\ \% = 10^2 \times (1 - m_{dry}/m)$ where m_{dry} is the dry mass of the hydrogel.

3. Results and discussion

3.1. Rheological properties

Three series of gelation experiments were conducted by fixing the amount of AMPS at 50 wt%, as compiled in Table 1. In the 1st set, Laponite nanoparticles between 1 and 15 wt% were added into the AMPS solution while in the 2nd set, BAAm instead of Laponite was included as a chemical cross-linker. In the 3rd set, both 15 wt% Laponite and BAAm at various amounts were added to generate hybrid cross-linked PAMPS hydrogels. In the following, gel-forming systems prepared using Laponite or BAAm are denoted as NC-*x* and BAAm-*y*, respectively, where *x* and *y* are Laponite (in wt%) and BAAm (in mol%) contents in the feed, respectively (Table 1). Moreover, the systems prepared using both Laponite and BAAm are denoted as hybrid-*x*/*y*.

We first conducted initiator-free polymerization of AMPS without any additive by heating aqueous 50 wt% AMPS solution from 25 to 80 °C at a rate of 1.8 °C·min^{-1}, and then keeping at this temperature for 18 h. Fig. 1a shows the storage G' and loss moduli G'' of the AMPS solution during the heating period plotted against the temperature. Above 45 °C, G' rapidly increases with increasing temperature and becomes equal to G'' at 54 °C indicating a transition from dilute to semi-dilute regime of PAMPS solution. Thus, in accord with the previous report [16], polymerization of AMPS could be initiated without an external initiator. Previous works show that some acrylic monomers such as acrylic acid and methacrylic acid undergo self-initiated photopolymerization or thermal polymerization [25,26]. Because AMPS does not self-polymerize when its H^+ is substituted by Na^+ [16], the presence of H^+ ions seems to be responsible for initiator-free polymerization of AMPS. After a reaction time of 24 h, frequency sweep tests were conducted on PAMPS hydrogels at 25 °C. Fig. 1b shows G', G'' and the loss factor tan δ ($= G''/G'$) at a strain amplitude γ_o of 0.01 plotted against the angular frequency ω. G' is larger than G'' over the entire range of frequency while tan δ is above 0.1, which is typical for a weak gel. Indeed, PAMPS hydrogel exhibited poor mechanical properties, e.g. its tensile strength and Young's modulus were 11 ± 1 and 9 ± 2 kPa, respectively, and it easily dissolved in water.

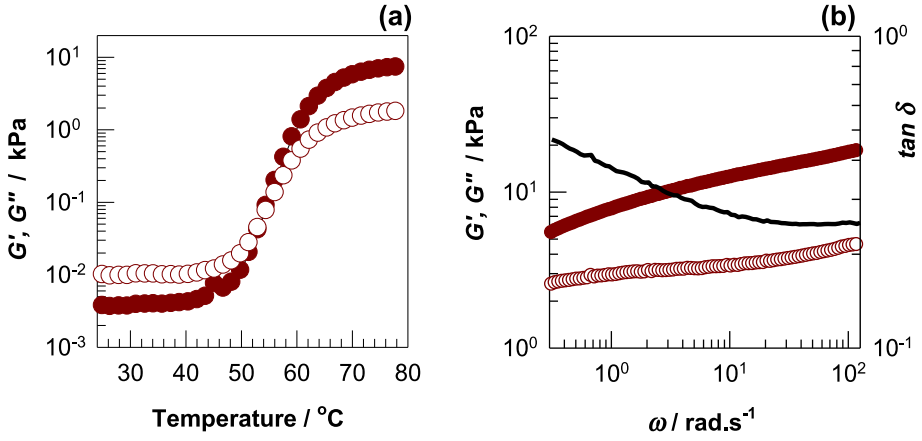

Fig. 1. (a) G' (filled symbols) and G'' (open symbols) of 50 wt% AMPS solution during heating from 25 to 80 °C shown as a function of temperature. $\omega = 6.3$ rad·s^{-1}. $\gamma_o = 0.01$. (b) G' (filled symbols), G'' (open symbols), and tan δ (lines) of PAMPS hydrogel after a reaction time of 24 h shown as a function of frequency ω. Temperature = 25 °C (c). $\gamma_o = 0.01$.

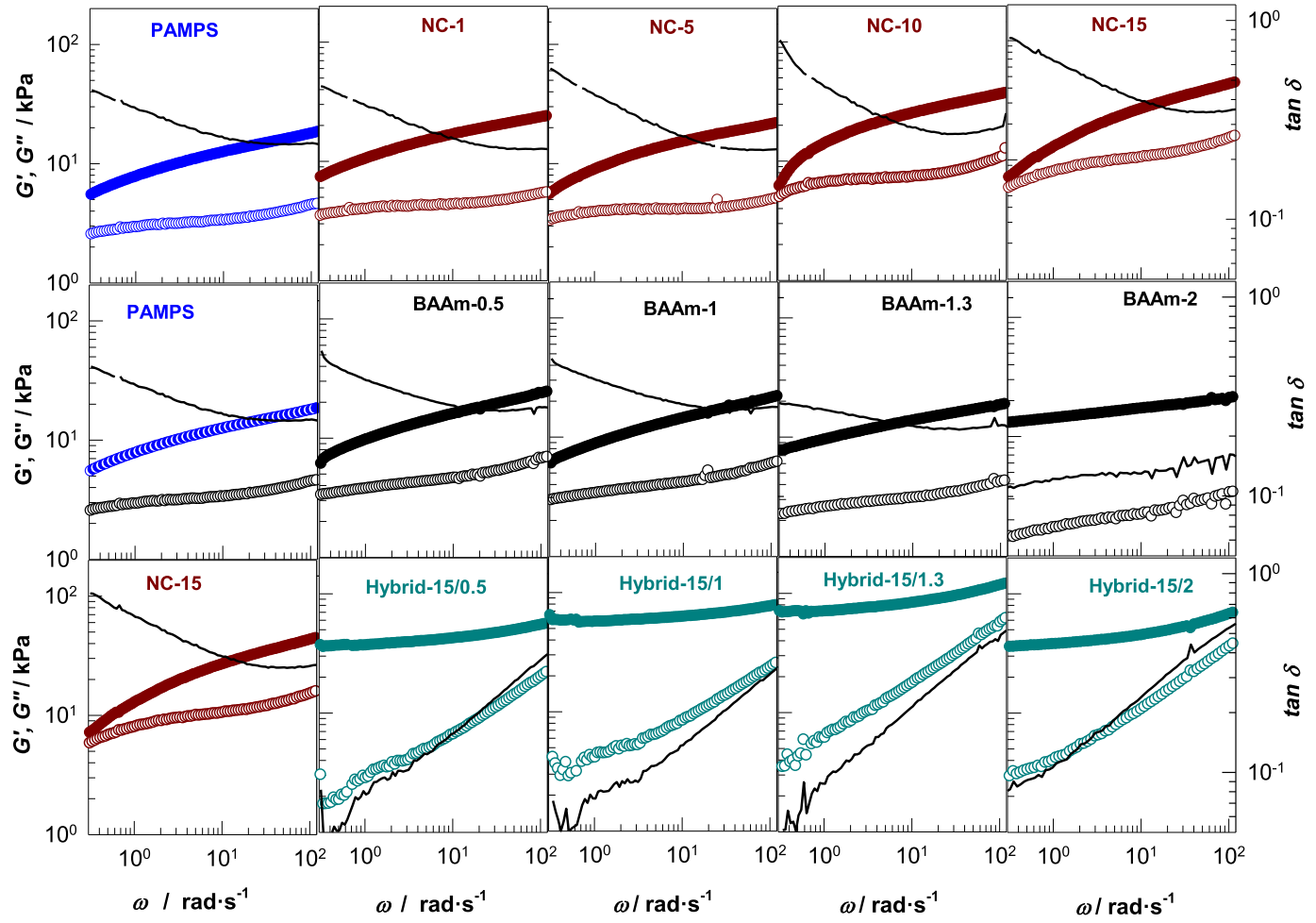

Fig. 2. G' (filled symbols), G'' (open symbols), and *tan* δ (lines) of NC-*x*, BAAm-*y*, and hybrid-15/*y* hydrogels at 25 °C shown as a function of frequency ω. $\gamma_o = 0.01$.

To render PAMPS hydrogel water-insoluble and to increase its mechanical strength, we included Laponite nanoparticles and the chemical cross-linker BAAm separately or together into the reaction system. Fig. 2 shows frequency dependences of G' (filled symbols), G'' (open symbols), and tan δ (lines) of NC-*x*, BAAm-*y*, and hybrid-15/*y* hydrogels, respectively, prepared at various Laponite and BAAm contents. Although the storage modulus G' and hence the cross-link density of NC's slightly increases with increasing amount of Laponite (Fig. 2, Table 1), the loss factor tan δ also increases indicating that the physical PAMPS gel becomes more viscous after incorporation of the nanoparticles into the physical network. Indeed, all NC's were soluble in water as those prepared in the absence of Laponite. This unexpected behavior could be related to the repulsive interactions between the negatively charged surface of the nanoparticles and PAMPS chains, as observed before in hydrogels formed by in-situ copolymerization of AMPS and acrylamide in Laponite dispersions [23,27]. Similar to the NC's, gel forming systems containing BAAm cross-linker lead to the formation of weak gels (Fig. 2b) and, except the one prepared using 2 mol% BAAm, they all are soluble in water (Table 1). We have to mention that, below a critical cross-linker (divinyl monomer) concentration, cross-linking copolymerization of vinyl/divinyl monomers results in water soluble polymers [28,29]. This critical concentration is

generally much higher than the theoretical one due to the effects of cyclization and multiple cross-linking reactions as well as due to the reduced reactivity of pendant vinyl groups on the growing radicals. For the present gelation system, 2 mol% BAAm is needed to obtain a chemically cross-linked PAMPS hydrogel, while at lower BAAm contents, BAAm does not form elastically effective cross-links between PAMPS chains and hence, water-soluble physical gels could be obtained.

However, hybrid-cross-linked hydrogels prepared by the addition of both Laponite and BAAm exhibit significantly improved elastic properties (Fig. 2 and Table 1). The storage modulus G' shows a plateaulike behavior in the low-frequency range and the height of the plateau increases with increasing BAAm concentration. Plateau storage modulus G' of hybrids is about one order of magnitude higher than that of their components, i.e., NC- and BAAm-hydrogels, and the loss factor tan δ attains values below 0.1 at low frequencies. Moreover, all hybrids were insoluble in water with a gel fraction W_g around unity (Table 1), indicating that the cross-links in hybrid hydrogels resist the expansion of PAMPS chains in water. The results thus reveal that Laponite and BAAm separately are ineffective for the improvement of PAMPS hydrogel properties while their combination produces water-insoluble hydrogels with a high modulus.

The results can be explained by considering the interactions between the components of the gelation system. Previous work shows that non-ionic monomers such as *N*-isopropylacrylamide, *N*,*N*-dimethylacrylamide, and acrylamide effectively surround the surface of Laponite particles in aqueous suspensions [19–22,30]. After gelation, a large number of non-ionic polymer chains are aggregated on the surface of clay particles forming multiple hydrogen bonding with clay, which is responsible for the extraordinary mechanical properties of nanocomposite hydrogels. In contrast, anionic monomer AMPS cannot surround the particles due to its repulsive interactions with the negatively charged particle surfaces, which prevents hydrogen bonding between PAMPS and clay. Thus, because Laponite surfaces do not act as multifunctional cross-link zones of PAMPS chains, weak physical gels could be obtained from AMPS monomer. However, when BAAm is added in the gelation system containing Laponite and AMPS, non-ionic BAAm molecules surrounding the particles act like bridges between the particle surfaces and AMPS and hence enhance clay-polymer interactions leading to improved mechanical properties of hybrid hydrogels.

This finding is also highlighted in Fig. 3a–c where the frequency dependences of G', G'', and tan δ of hybid-15/2 hydrogel together with its component hydrogels, namely NC-15 and BAAm-2 are shown. Solid and dashed gray curves in Fig. 3a represent the theoretical G' and tan δ of hybrid-15/2, respectively, calculated by summing up the dynamic moduli of its component hydrogels. At $\omega > 6$ rad·s^{-1}, calculated G' is close to its experimental value indicating that both the physical and chemical cross-links are effective in the hybrid network structure. At lower frequencies, a positive deviation from the calculated G' appears which can be attributed to the reduced mobility of chemically cross-linked PAMPS chains increasing the lifetime of H-bonds between PAMPS and Laponite. This explanation is in accord with much lower tan δ of the hybrids as compared to its calculated value (Fig. 3a). For instance, at $w = 0.3$ rad·s^{-1}, tan δ is 0.05, indicating that the hybrid hydrogel at this time scale belongs to the category of strong gels, while the calculated value of *tan* δ is 0.4, typical for a weak gel (Fig. S1).

Another point seen in Fig. 3a is increasing G'' and tan δ (solid blue line) with increasing frequency revealing energy dissipation at short experimental time scales. Such a significant increase of G'' with rising frequency has been reported before in polysaccharide gels with strong hydrogen bonding interactions, such as sodium alginate - poly(*N*-isopropylacrylamide) (PNIPA) [31], hyaluronic acid-graft-PNIPA [32], methyl cellulose [33], and hyaluronic acid [34]. The appearance of a similar viscoelastic behavior in hybrid-PAMPS hydrogels is attributed to the strong intermolecular hydrogen bonding interactions between chemically cross-linked PAMPS and Laponite nanoparticles contributing to the gel elasticity at a low frequency. Increasing frequency progressively breaks H-bonds so that strong hydrogel transforms into a weak one. This also means that heating the hybrid hydrogels would break H-bonds existing at short frequencies. The dashed blue curve in Fig. 3a representing ω-dependence of tan δ measured at 40 °C indeed reveals that tan δ is close to the calculated value indicating that most of H-bonds are broken at the elevated temperature.

Stress-relaxation experiments are another mean of studying the dynamic properties of the hydrogels. Fig. 4a–c show the relaxation modulus $G(t)$ of the hydrogels during the first second of relaxation following a step strain of 5%. The hydrogels exhibit a two-step relaxation response consisting a fast relaxation at time t shorter than 0.2 s and slow relaxation at longer times. The fact that all hydrogels exhibit relaxation reveals finite lifetimes of their apparent cross-links and energy dissipation. Fig. 4d–f show double-logarithmic plots of $G(t)$, normalized with respect to the modulus G_R at $t = 0$, as a function of time t up to 100 s for NC-, BAAm-, and hybrid-hydrogels, respectively, formed at various Laponite and BAAm contents. The measurements were performed at 5% strain which is in the linear regime for all hydrogels (Fig. S2). For all hydrogels, $G(t)$ decreases with time but never goes to zero over the duration of the relaxation tests.

The strongest time-dependence of the relaxation modulus G(t) was observed in NC-hydrogels, with $G(t)$ being a mirror image of $G'(w)$ (Fig. 2a). For Laponite contents below 10 wt%, all data could be fitted using the stretched exponential function [35–38]:

$$G(t) = G_R \exp(-(t/\tau)^{\beta}) \quad (1)$$

with an exponent $\beta = 0.25 \pm 0.05$, where τ is the lifetime of the physical crosslinks. At larger amount of Laponite, the data below 1 s could also be fitted to the stretched exponential function with the same exponent while at longer time scales a power law behavior similar to the critical gel appears, $G(t) \sim t^n$ where $n = -0.83 \pm 0.05$. The solid red curves in Fig. 4d–f are best fit curves using Eq. (1). The inset to

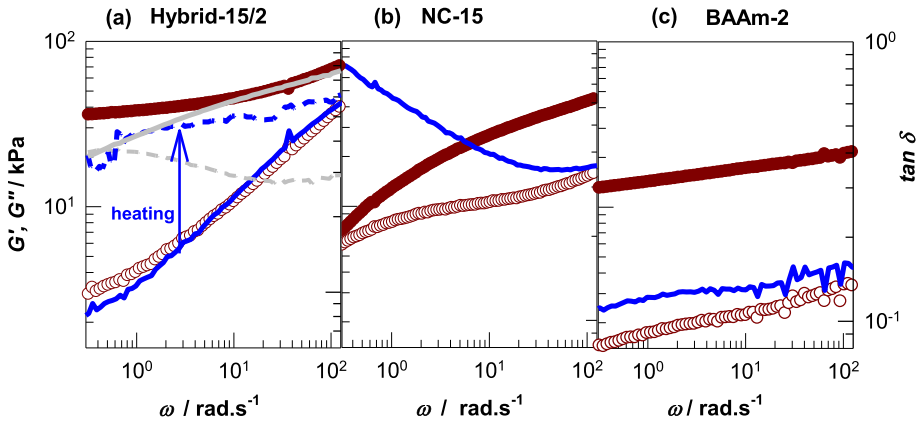

Fig. 3. G' (filled symbols), G'' (open symbols), and tan δ (solid blue lines) of hybrid-15/2 (a), NC-15 (b), and BAAm-2 hydrogels (c) shown as a function of frequency ω. $\gamma_o = 0.01$. The solid and dashed gray curves in Fig. 3a are G' and tan δ, respectively, calculated by summing up G' and G'' of NC-15 and BAAm-2 hydrogels. Temperature = 25 °C. Dashed blue curve in Fig. 3a represents tan δ values measured at 40 °C. (For interpretation of the references to colour in this figure legend, the reader is referred to the web version of this article.)

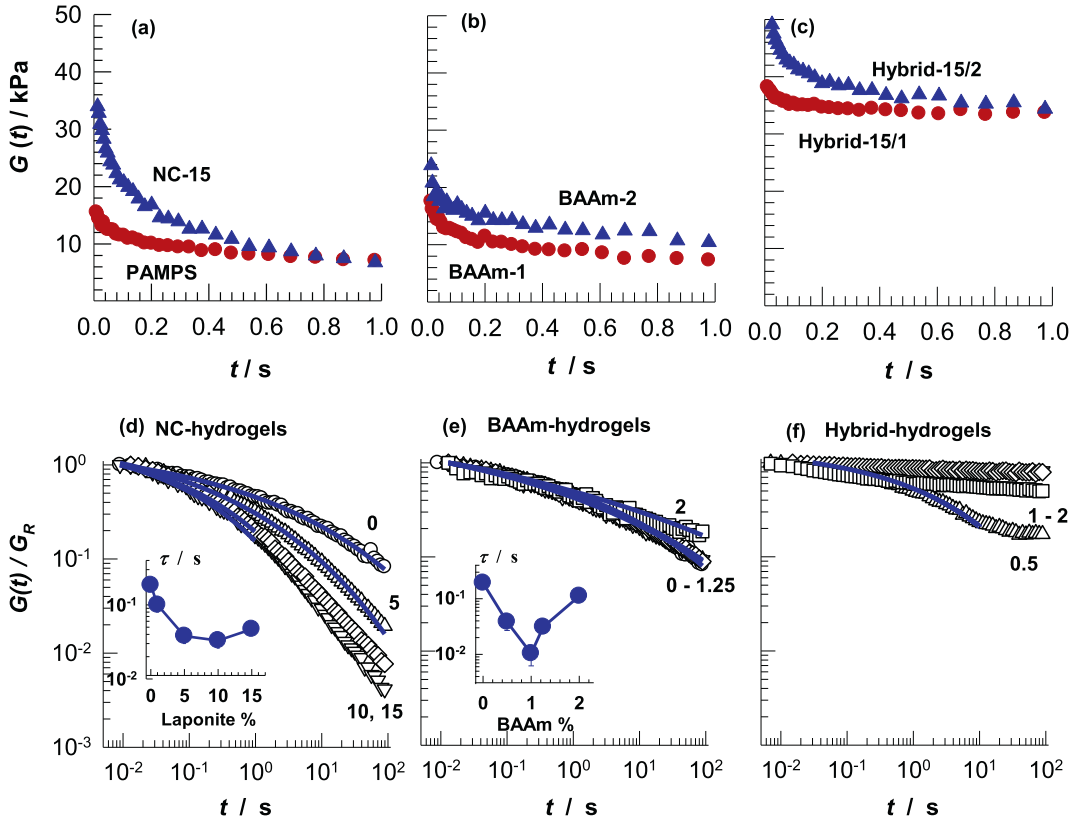

Fig. 4. (a–c): Relaxation modulus $G(t)$ during a relaxation time of 1 s for PAMPS, NC-15, BAAm-1, BAAm-2, and resulting hybrid-hydrogels. Strain = 5%. (d–f): $G(t)$ normalized with respect to the Rouse modulus G_R as a function of time t for NC- (d), BAAm- (e), and hybrid-hydrogels (f). (d) Laponite = 0 (○), 5 (Δ), 10 (▽), and 15 wt% (⋄). (e, f) BAAm = 0 (○), 0.5 (Δ), 1.0 (▽), 1.25 (⋄), and 2 mol% (□). Strain = 5%. The curves are the best fits to Eq. (1). The insets show the lifetime τ of physical cross-links as functions of Laponite and BAAm contents.

Fig. 4d showing the lifetime τ of the physical cross-links calculated using Eq. (1) reveals formation of H-bonds with shorter lifetimes as the amount of Laponite is increased. A similar behavior was observed in BAAm-hydrogels (inset to Fig. 4e). Increasing amount of BAAm up to 1 mol% decreases the lifetime τ while it again increases at higher BAAm contents. In contrast, the hybrids with > 0.5 mol% BAAm exhibit only a slight time-dependent relaxation modulus supporting the existence of long-lived H-bonds in hybrid network structure.

3.2. Mechanical properties

Hydrogels were subjected to uniaxial tensile and compression tests at 24 ± 2 °C. Fig. 5 shows tensile stress-strain curves at a strain rate $\dot{\varepsilon}$ of 1 min^{-1} for PAMPS, BAAm-1, NC-15, and Hybrid-15/1 hydrogels. PAMPS hydrogel exhibits a Young's modulus of 9 ± 2 kPa and a very high extensibility, about 2600%. The stretchability of PAMPS hydrogel decreases from 2600 to 200% after incorporation of BAAm into the comonomer feed while in hybrid one, it further reduces to 13%. Simultaneously, Young's modulus E increases from 9 ± 2 to 70 ± 3 and 350 ± 44 kPa indicating increasing effective crosslink density of the hydrogels (inset to Fig. 5). We have to mention that the hybrids formed at higher BAAm contents were mechanically stronger than Hybrid-15/1 shown in Fig. 5 but they were too slippery to obtain meaningful tensile test results. Therefore, the mechanical properties of all hydrogels were compared by uniaxial compression tests.

Fig. 6a–c show compressive stress-strain curves of NC-15, BAAm-2, and Hybrid-15/2 hydrogels, respectively, at various strain rates $\dot{\varepsilon}$. For NC-15 hydrogel, a strong strain rate dependence of the stress-strain curves is seen with a significant increase of the compressive strength at high rates. In contrast, BAAm-2 hydrogel exhibits a weak strain rate sensitivity and a low compressive strength. Hybrid-15/2 hydrogel

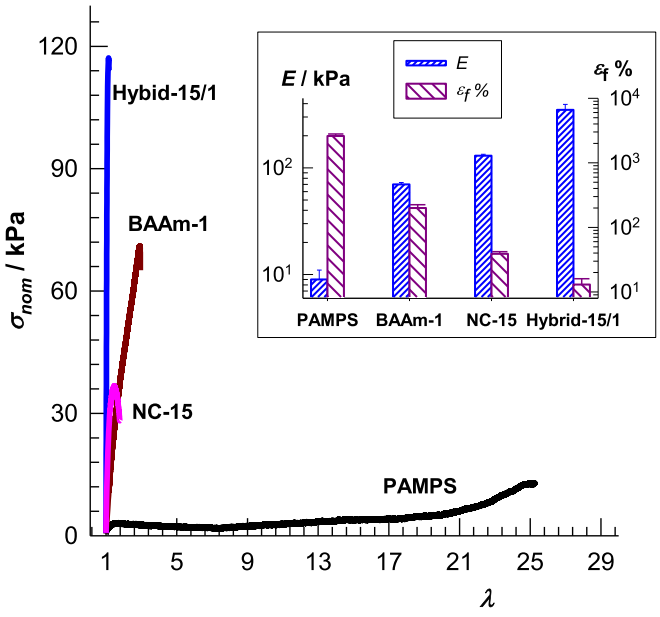

Fig. 5. Tensile stress – strain curves of PAMPS, NC-15, BAAm-1 and hybrid-15/1 hydrogels as the dependence of the nominal stress σ_{nom} on the deformation ratio λ. $\dot{\varepsilon}$ = 1 min^{-1}. The inset shows the Young's modulus E and stretch at break ε_f of the hydrogels.

which is a combination of NC-5 and BAAm-2 also exhibits a weak strain rate dependence but it is the mechanically strongest hydrogel overall rates. Fig. 7a shows strain rate dependences of Young's modulus E and compressive strength σ_f of the precursor NC-15 and BAAm-hydrogels

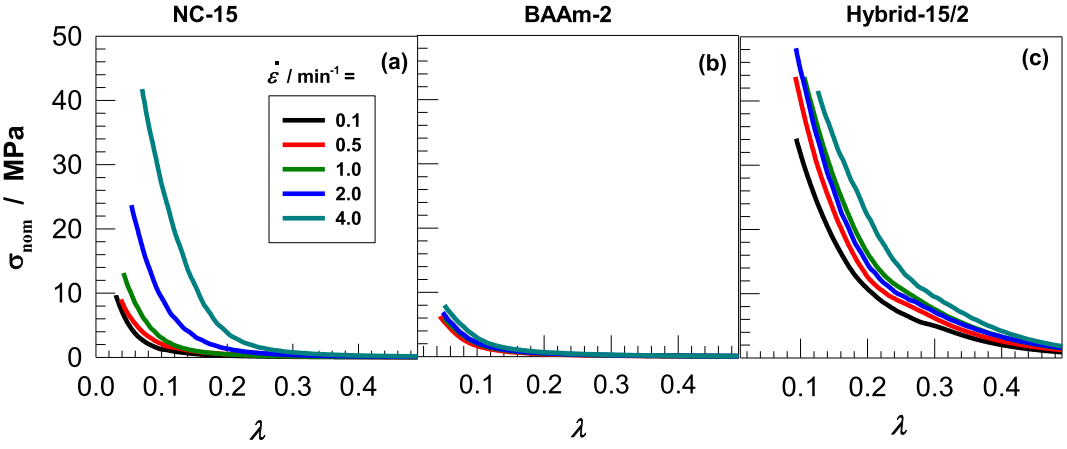

Fig. 6. Compressive stress – strain curves of NC-15 (a), BAAm-2 (b), and Hybrid-15/2 hydrogels (c) at various strain rates $\dot{\varepsilon}$ indicated.

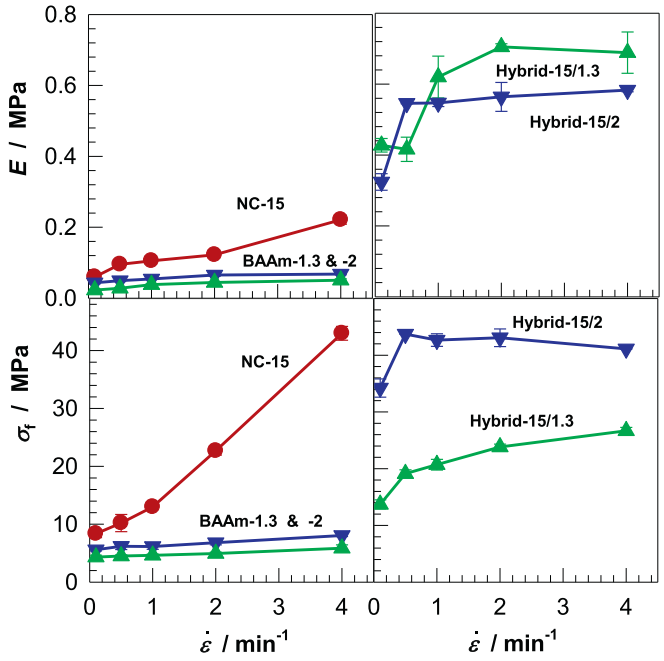

Fig. 7. Young's modulus E (upper panel) and compressive strength σ_f (bottom panel) of hybrid-hydrogels (right panel) and their component hydrogels (left panel) plotted against the strain rate $\dot{\varepsilon}$.

Table 2
Compressive modulus E and the fracture stress σ_f of hybrid-15/1.3 and -15/2 hydrogels together with their component hydrogels at two strain rates. Standard deviations are given in parenthesis.

Code	E/kPa		σ_f/MPa	
	at 0.5 min^{-1}	at 4 min^{-1}	at 0.5 min^{-1}	at 4 min^{-1}
NC-15	95 (10)	221 (13)	10.2 (1.5)	43 (1)
BAAm-1.3	28 (2)	51 (4)	4.5 (0.2)	5.9 (0.6)
BAAm-2	49 (3)	68 (2)	6.2 (0.6)	8.1 (0.2)
Hybrid-15/1.3	416 (34)	690 (58)	19.1 (0.7)	27 (1)
Hybrid-15/2	546 (8)	583 (5)	44 (2)	41 (1)

(left panel), and the resulting hybrids (right panel). E and σ_f of the hydrogels at two different strain rates are also compiled in Table 2. Hybrid-hydrogels exhibit a modulus E between 400 and 700 kPa at strain rates $\dot{\varepsilon}$ above 0.1 min^{-1}, which is about 15- and 4-fold higher than the precursor NC- and BAAm-hydrogels indicating increasing number of effective cross-links when both Laponite and BAAm are incorporated into the physical PAMPS network. Comparison of the swelling behavior of the hydrogels also reflects significant difference in the cross-link density of BAAm-2 and hybrid-15/2 hydrogels. Fig. 8a shows relative weight swelling ratio m_{rel} of BAAm-2, and hybrid 15/y hydrogels plotted against the time of swelling in water while Fig. 7b shows the images of BAAm-2 and hybrid-15/2 hydrogel specimens before and after equilibrium swelling in water. The mass of BAAm-2 hydrogel sample 160-fold increases upon swelling in water which is 40 times larger than the mass increase observed in hybrid-15/2 gel sample. Moreover, increasing BAAm content of hybrids from 0.5 to 2 mol% decreases the swelling ratio m_{rel} from 7.4 to 5.3 indicating increasing cross-link density of the hydrogels.

All the mechanical properties of the hydrogels reported so far are related to their as-prepared states. Because NC- and BAAm-hydrogels, except BAAm-2, are soluble in water (Table 1), we can only compare the mechanical characteristics of BAAm-2 with the resulting hybrid-15/2 hydrogel in their equilibrium swollen states in water. Fig. 9a shows compressive stress-strain curves of swollen BAAm-2 and hybrid-15/2 hydrogels while Fig. 9b compares their Young's modulus and compressive strength. It is seen that the mechanical performance of the hydrogels significantly decreases after their swelling due to the dilution of PAMPS chains. However, hybrid-15/2 exhibits 6-fold larger modulus (48 ± 4 kPa) and 5-fold larger compressive strength (126 ± 14 kPa) as compared to BAAm-2 precursor.

3.3. Self-healing properties

Supramolecular and hybrid network structures of the hydrogels suggest that they would possess the ability to self-heal after creating a damage. To find out whether the cross-links making the hydrogel network would break reversibly or irreversibly under an external load, we performed cyclic compression tests at a strain rate $\dot{\varepsilon}$ of 1 min^{-1}. Fig. 10a–d show loading/unloading cycles of PAMPS, NC-15, BAAm-1, and Hybrid-15/1 hydrogels, respectively, conducted under increased maximum strain ε_{max} from 20 to 80% compression with a waiting time of 5 min between cycles. Loading and unloading curves are indicated by solid and dashed lines, respectively. The general trend is that the unloading curve of each cycle follows a different path from the loading curve with a smaller area under the curve, indicating dissipation of energy due to breaking of intermolecular bonds. Below the maximum strain ε_{max} of 80%, each loading curve follows the path of the previous loading demonstrating that the intermolecular bonds broken under stress are reformed during the waiting time of 5 min. However, the loading curve for ε_{max} = 80% (solid blue line) deviates from the previous loading and the extent of deviation increases in the order of BAAm-1 < Hybrid-15/1 < PAMPS < NC-15. The results thus suggest existence of both reversibly and irreversibly broken bonds in the

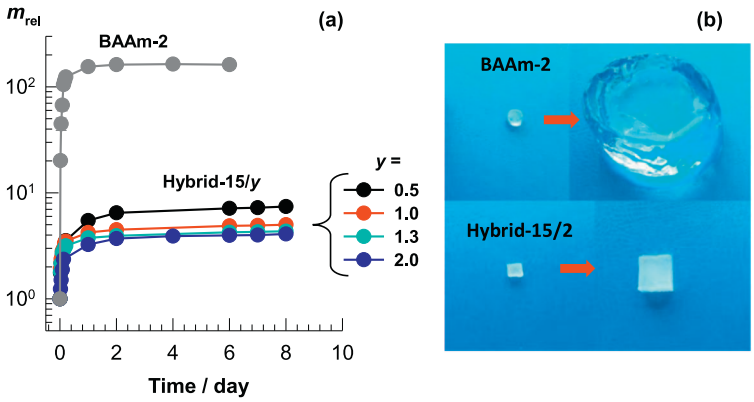

Fig. 8. (a): Relative weight swelling ratio m_{rel} of BAAm-2, and hybrid 15/y hydrogels plotted against the time of swelling in water. BAAm contents y (in mol%) are indicated. (b): Images of BAAm-2 and hybrid-15/2 hydrogel specimens before and after equilibrium swelling in water.

hydrogels.

The energy U_{hys} dissipated during the compression cycles was estimated from the area between the loading and unloading curves using the equation:

$$U_{hys} = \int_0^{\varepsilon_{max}} \sigma_{nom}\, d\varepsilon - \int_{\varepsilon_{max}}^0 \sigma_{nom}\, d\varepsilon \quad (2)$$

while the resilience R representing the ability of a hydrogel to deform reversibly without dissipation of energy was calculated from the ratio of the areas below the unloading to the loading curves, i.e.,

$$R = \frac{\int_{\varepsilon_{max}}^0 \sigma_{nom}\, d\varepsilon}{\int_0^{\varepsilon_{max}} \sigma_{nom}\, d\varepsilon} \quad (3)$$

Hysteresis energy U_{hys} and resilience R of the hydrogels are plotted in Fig. 10e as a function of the maximum strain ε_{max}. Hybrid hydrogel exhibits both the highest resilience R and hysteresis energy U_{hys} among the hydrogels. Because R corresponds to the recovered energy while the dissipated energy U_{hys} is proportional to the number of broken bonds, the number of bonds broken under strain is largest in hybrid hydrogel but most of these bonds are reformed after the cycle. Although NC-15 hydrogel also exhibits a large hysteresis, its resilience is the lowest revealing the occurrence of an irreversible damage.

Self-healing ability of the hydrogels was also macroscopically investigated by cutting the gel specimens into two parts, and then merging the cut surfaces by pressing together. Self-healing tests were conducted on PAMPS, NC-15, BAAm-1, and hybrid-15/1 hydrogels. The hydrogels prepared without Laponite, that is, both PAMPS and BAAm-1 could be healed at room temperature (24 ± 2 °C) after a healing time of 24 h (Fig. S3). However, healing in the gel specimens containing Laponite could only be induced by heating the cut surfaces above the room temperature. In the following, healing tests of NC-15 and hybrid-15/1 hydrogels were conducted at 50 °C for 24 h. To quantify the healing efficiency, tensile tests at a strain rate of 1 min^{-1} were conducted on both virgin and healed hydrogel samples. For all hydrogels studied, we observed that the second damage always occurred in the healed region of the gel specimens revealing that the original network structure cannot be completely recovered after the healing process.

Fig. 11a shows stress-strain curves of virgin and healed PAMPS, NC-15, BAAm-1, and hybrid-15/1 hydrogels. It is seen that the fracture stress of all healed gel samples is lower than that of the virgin ones. Moreover, healed BAAm-1 and hybrid-15/1 hydrogels exhibit larger elongation at break as compared to virgin ones, likely because of the lower cross-link density of the healed samples contributing to the extensibility of the network chains. In Fig. 11b, Young's modulus E and compressive strength σ_f of virgin (filled bars) and healed hydrogel samples (open bars) together with the corresponding healing efficiencies ε_{eff} (line and symbols) are compiled for the hydrogels studied. The highest modulus and strength after healing was observed in hybrid hydrogels. The healing efficiencies of the hydrogels with respect to the modulus and strength are between 16 and 78 and 37–58%, respectively, and they decrease in the order PAMPS > BAAm-1 > Hybrid-15/1 > NC-15. Thus, although hybrid hydrogel exhibits a much higher modulus (348 vs 129 kPa) and strength (109 vs 35 kPa) as compared to the NC-hydrogel, it exhibits a better healing performance.

4. Conclusions

We described a simple strategy to prepare mechanically strong PAMPS hydrogels with self-healing ability. Initiator-free polymerization of AMPS in aqueous solutions in the presence of Laponite nanoparticles and BAAm cross-linker produces hybrid-cross-linked hydrogels with

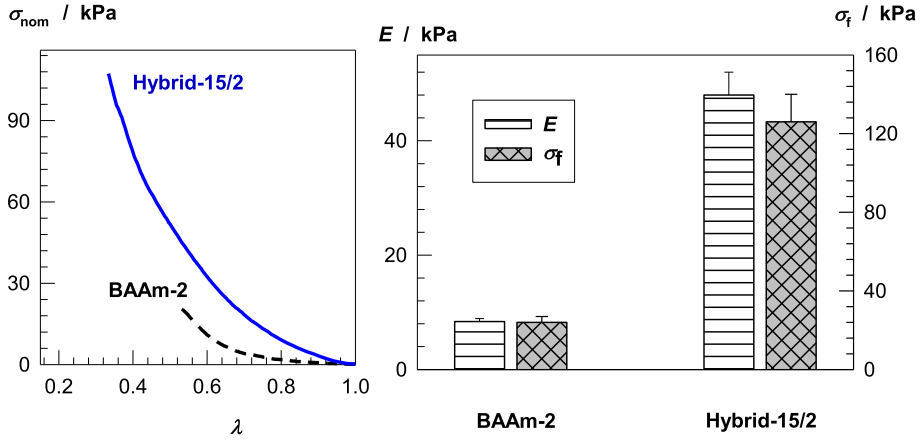

Fig. 9. (a): Compressive stress – strain curves of BAAm-2 and Hybrid-15/2 hydrogels in their equilibrium swollen states in water. $\dot{\varepsilon}$ = 1 min^{-1}. (b): Young's modulus E and fracture stress σ_f of swollen BAAm-2 and Hybrid-15/2 hydrogels.

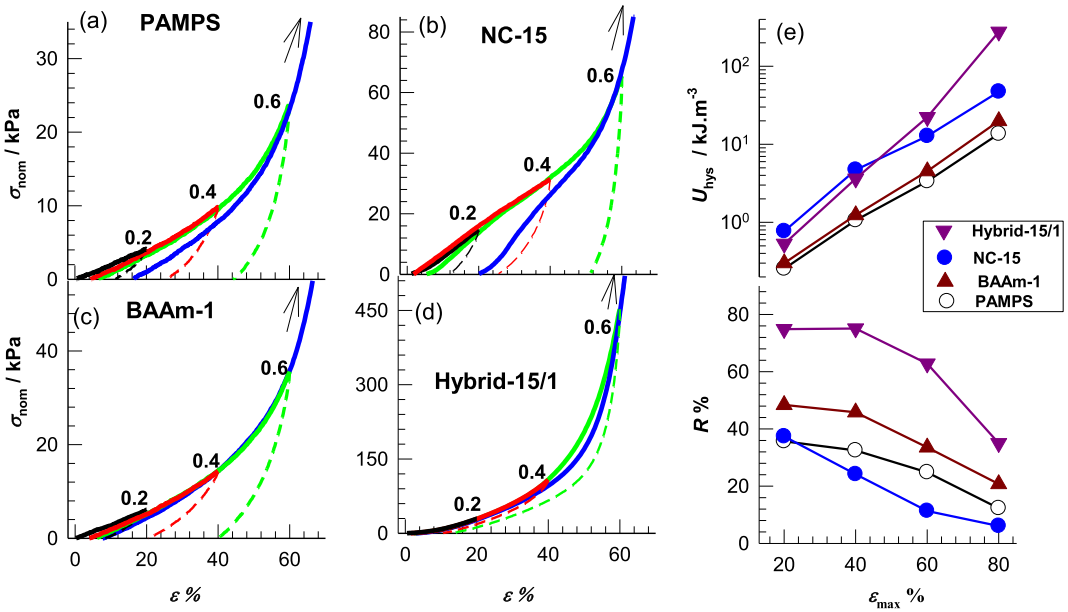

Fig. 10. (a–d): Loading/unloading compression cycles for PAMPS (a), NC-15 (b), BAAm-1 (c), Hybrid-15/1 hydrogels (d). The tests were conducted with increasing maximum strain ε_{max} from 20 to 80%, as indicated. Loading and unloading curves are shown by solid and dashed lines, respectively. $\dot{\varepsilon} = 1\ min^{-1}$. Wait time between cycles = 5 min. (e): ε_{max} dependences of the hysteresis energy U_{hys} and resilience R for PAMPS (○), NC-15 (●), BAAm-1 (▲), and Hybrid-15/1 hydrogels (▼).

excellent mechanical prope rties. To elucidate the individual effects of Laponite and BAAm on the hydrogel properties, the hydrogels were also prepared without any additive as well as after incorporating of Laponite and BAAm alone into the physical network. AMPS polymerization without any additive leads to highly stretchable hydrogels with an elongation at break of 2600%. However, PAMPS hydrogels easily dissolve in water due to the weak inter-chain hydrogen bonds. Addition of Laponite or BAAm separately further weakens the hydrogen bonding interactions and hence produces weak and water-soluble hydrogels. In contrast, simultaneous incorporation of Laponite and BAAm into the physical network leads to hybrid cross-linked PAMPS hydrogels with superior mechanical properties. They exhibit a high modulus (~700 kPa), compressive strength (45 MPa at ~90% strain), good resilience, and self-healing. The strength of hybrid cross-linked PAMPS hydrogels is attributed to the strong interactions between chemically cross-linked PAMPS chains and nanoparticles. The hybrid approach presented here might enable preparation of mechanically strong nanocomposite hydrogels consisting of strongly or weakly charged polymer chains of different architecture.

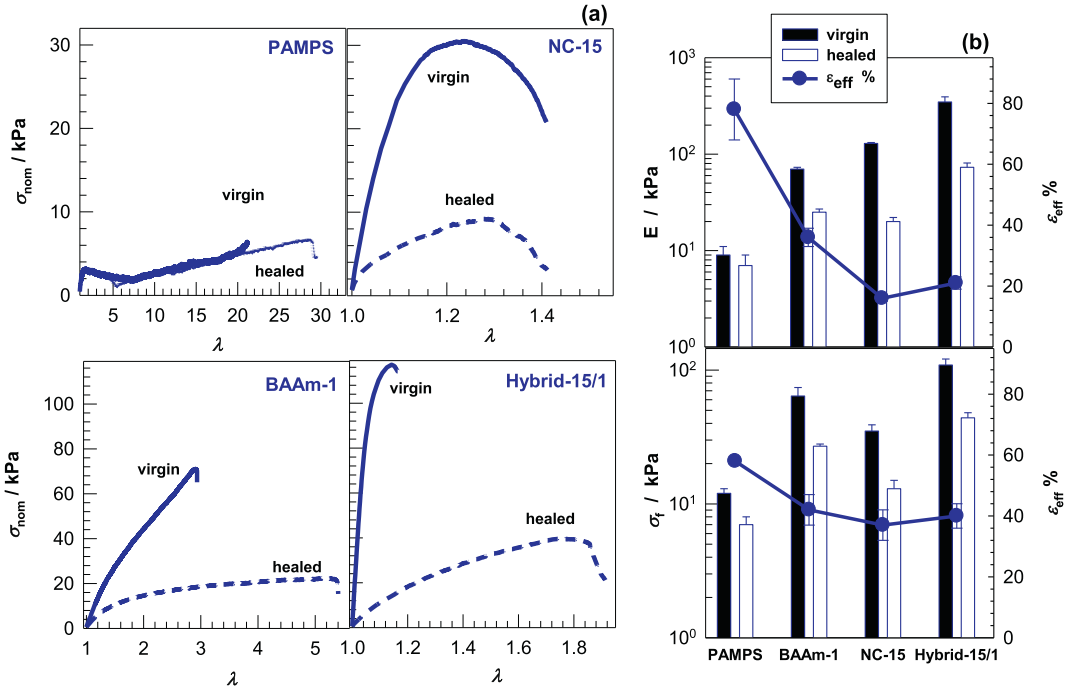

Fig. 11. (a): Stress-strain curves of virgin and healed PAMPS, NC-15, BAAm-1, and hybrid-15/1 hydrogels. (b): Young's modulus E and compressive strength σ_f of virgin (filled bars) and healed hydrogel samples (open bars), and their healing efficiencies ε_{eff} (symbols).

Acknowledgements

This work was supported by the Scientific and Technical Research Council of Turkey (TUBITAK), KBAG 114Z312. E.S. thanks TUBITAK-BIDEB for a PhD scholarship. O.O. thanks Turkish Academy of Sciences (TUBA) for the partial support.

Appendix A. Supplementary data

Supplementary data to this article can be found online at https://doi.org/10.1016/j.reactfunctpolym.2017.12.009.

References

[1] S. Durmaz, O. Okay, Acrylamide/2-acrylamido-2- methyl propane sulfonic acid sodium salt -based hydrogels: synthesis and characterization, Polymer 41 (2000) 3693–3704.
[2] F. Topuz, O. Okay, Macroporous hydrogel beads of high toughness and superfast responsivity, React. Funct. Polym. 69 (2009) 273–280.
[3] B. Boonkaew, P.M. Barber, S. Rengpipat, P. Supaphol, M. Kempf, J. He, V.T. John, L. Cuttle, Production with gamma irradiation creates silver nanoparticles and radical polymerization, J. Pharm. Sci. 103 (2014) 3244–3253.
[4] S. Beuermann, M. Buback, P. Hesse, T. Junkers, I. Lacik, Free-radical polymerization kinetics of 2acrylamido-2-methylpropanesulfonic acid in aqueous solution, Macromolecules 39 (2006) 509–516.
[5] L.W. Fisher, A.R. Sochor, J.S. Tan, Chain characteristics of poly(2-acrylamido-2-methylpropanesulfonate) polymers. 1. Light-scattering and intrinsic-viscosity studies, Macromolecules 10 (1977) 949–954.
[6] X. Liu, Z. Tong, O. Hu, Swelling equilibria of hydrogels with sulfonate groups in water and in aqueous salt solutions, Macromolecules 28 (1995) 3813–3817.
[7] Z. Tong, X. Liu, Swelling equilibria and volume phase transition in hydrogels with strongly dissociating electrolytes, Macromolecules 27 (1994) 844–848.
[8] C. Yang, Z. Liu, C. Chen, K. Shi, L. Zhang, X.-J. Ju, W. Wang, R. Xie, L.Y. Chu, Reduced graphene oxide-containing smart hydrogels with excellent electro-response and mechanical properties for soft actuators, ACS Appl. Mater. Interfaces 9 (2017) 15758–15767.
[9] A. Jones, D. Vaughan, Hydrogel dressings in the management of a variety of wound types: a review, J. Orthop. Nurs. 9 (2005) 1–11.
[10] J.P. Gong, T. Kurokawa, T. Narita, G. Kagata, Y. Osada, G. Nishimura, M. Kinjo, Synthesis of hydrogels with extremely low surface friction, J. Am. Chem. Soc. 123 (2001) 5582–5583.
[11] K. Nalampang, R. Panjakha, R. Molloy, B.J. Tighe, Structural effects in photo-polymerized sodium AMPS hydrogels crosslinked with poly(ethylene glycol) diacrylate for use as burn dressings, J. Biomater. Sci. Polym. Ed. 24 (2013) 1291–1304.
[12] P. Calvert, Hydrogels for soft machines, Adv. Mater. 21 (2009) 743–756.
[13] X. Zhao, Multi-scale multi-mechanism design of tough hydrogels: building dissipation into stretchy networks, Soft Matter 10 (2014) 672–687.
[14] Y. Tanaka, K. Fukao, Y. Miyamoto, Fracture energy of gels, Eur. J. Phys. E 3 (2000) 395–401.
[15] H.R. Brown, A model of the fracture of double network gels, Macromolecules 40 (2007) 3815–3818.
[16] A. Xing, L. Li, T. Wang, Y. Ding, G. Liu, G. Zhang, A self-healing polymeric material: from gel to plastic, J. Mater. Chem. A 2 (2014) 11049–11053.
[17] P. Mongondry, J.-F. Tassin, T. Nicolai, Revised state diagram of Laponite dispersions, J. Colloid Interface Sci. 283 (2005) 397–405.
[18] P. Mongondry, T. Nicolai, J.-F. Tassin, Influence of pyrophosphate or polyethylene oxide on the aggregation and gelation of aqueous Laponite dispersions, J. Colloid Interface Sci. 275 (2004) 191–196.
[19] K. Haraguchi, T. Takehisa, Nanocomposite hydrogels: a unique organic–inorganic network structure with extraordinary mechanical, optical, and swelling/de-swelling properties, Adv. Mater. 14 (2002) 1120–1124.
[20] K. Haraguchi, R. Farnworth, A. Ohbayashi, T. Takehisa, Compositional effects on mechanical properties of nanocomposite hydrogels composed of poly(*N*,*N*-dimethylacrylamide) and clay, Macromolecules 36 (2003) 5732–5741.
[21] A. Klein, P.G. Whitten, K. Resch, G. Pinter, Nanocomposite hydrogels: fracture toughness and energy dissipation mechanisms, J. Polym. Sci. B Polym. Phys. 53 (2015) 1763–1773.
[22] O. Okay, W. Oppermann, Polyacrylamide - clay nanocomposite hydrogels: rheological and light scattering characterization, Macromolecules 40 (2007) 3378–3387.
[23] J. Du, P. Chen, A. Adalati, S. Xu, R. Wu, J. Wang, C. Zhang, Preparation and mechanical properties of a transparent ionic nanocomposite hydrogel, J. Polym. Res. 21 (2014) 541 (1–6).
[24] U. Gulyuz, O. Okay, Self-healing poly(acrylic acid) hydrogels with shape memory behavior of high mechanical strength, Macromolecules 47 (2014) 6889–6899.
[25] H. Wang, H.R. Brown, Self-initiated photopolymerization and photografting of acrylic monomers, Macromol. Rapid Commun. 25 (2004) 1095–1099.
[26] M. Panagiotopoulou, S. Beyazit, S. Nestora, K. Haupt, B.T.S. Bui, Initiator-free synthesis of molecularly imprinted polymers by polymerization of self-initiated monomers, Polymer 66 (2015) 43–51.
[27] P. Chen, S. Xu, R. Wu, J. Wang, R. Gu, J. Du, A transparent Laponite polymer nanocomposite hydrogel synthesis via in-situ copolymerization of two ionic monomers, Appl. Clay Sci. 72 (2013) 196–200.
[28] W. Funke, O. Okay, B. Joos-Muller, Microgels- intramolecularly crosslinked macromolecules with a globular structure, Adv. Polym. Sci. 136 (1998) 139–234.
[29] O. Okay, M. Kurz, K. Lutz, W. Funke, Cyclization and reduced pendant vinyl group reactivity during the free-radical crosslinking polymerization of 1,4-divinylbenzene, Macromolecules 28 (1995) 2728–2737.
[30] K. Haraguchi, K. Uyama, H. Tanimoto, Self-healing in nanocomposite hydrogels, Macromol. Rapid Commun. 32 (2011) 1253–1258.
[31] M. Teodorescu, M. Andrei, G. Turturică, P.O. Stănescu, A. Zaharia, A. Sârbu, Novel thermoreversible injectable hydrogel formulations based on sodium alginate and poly(*N*-isopropylacrylamide), Int. J. Polym. Mater. Polym. Biomater. 64 (2015) 763–771.
[32] M. D'Este, M. Alini, D. Eglin, Single step synthesis and characterization of thermoresponsive hyaluronan hydrogels, Carbohydr. Polym. 90 (2012) 1378–1385.
[33] M. Kundu, S. Mallapragada, R.C. Larock, P.P. Kundu, Rheological properties of methylcellulose aqueous gels under dynamic compression: frequency sweep and validity of scaling law, J. Appl. Polym. Sci. 117 (2010) 2436–2443.
[34] B. Tavsanli, O. Okay, Preparation and fracture process of high strength hyaluronic acid hydrogels cross-linked by ethylene glycol diglycidyl ether, React. Funct. Polym. 109 (2016) 42–51.
[35] J. Hao, R.A. Weiss, Viscoelastic and mechanical behavior of hydrophobically modified hydrogels, Macromolecules 44 (2011) 9390–9398.
[36] G. Williams, D.C. Watts, Non-symmetrical dielectric relaxation behaviour arising from a simple empirical decay function, Trans. Faraday Soc. 66 (1970) 80–85.
[37] A.A. Gurtovenko, Y.Y. Gotlib, Dynamics of inhomogeneous cross-linked polymers consisting of domains of different sizes, J. Chem. Phys. 115 (2001) 6785–6793.
[38] T.S.K. Ng, G.H. McKinley, Power law gels at finite strains: the nonlinear rheology of gluten gels, J. Rheol. 52 (2008) 417–449.